Experimental Investigation on Acoustic Wave Generation due to Supersonic Hot Jet Impingement on an Inclined Flat Plate

I. Bahman-Jahromi[1, 2†], K. Ghorbanian[2] and M. Ebrahimi[1]

[1] *Aerospace Research Institute (Ministry of Science, Research and Technology), 14665-834, Tehran, Iran*
[2] *Aerospace Engineering Department, Sharif University of Technology, 11365-11155, Tehran, Iran*

†*Corresponding Author Email: bahman@ari.ac.ir*

ABSTRACT

In the present paper, noise generation due to supersonic hot jet impingement (M=1.4 and T_t=950 K) to an inclined flat plate is experimentally investigated. In general, four types of acoustic waves are defined for jet impingement: acoustic waves generated by the shear layer of the main jet (type-A), by the impingement region (type-B), by the shear layer of the wall/jet downstream of the impinging region (type-C), and tonal acoustic waves observed in normal impingement. An attempt is made to understand the sources of the noise of the impinging jet by comparing acoustic scalograms of the impinging and free jets at the far-field. It is determined that the type-C acoustic wave images are similar to the far-field scalogram images of the free jet at the same polar angles. Further, the type-B acoustic waves in oblique jet impingement have similar acoustic signature with tonal noise due to normal jet impingement.

Keywords: Hot jet impingement; Noise generation; Acoustic event; Feedback loop mechanism.

NOMENCLATURE

C_a	acoustic wave velocity	T	temperature
C_i	large scale structure convection velocity	T_t	stagnation temperature
D	nozzle exit diameter	t	time
f_N	frequency associated with the feedback loop	U	jet velocity
		V_{is}	incident shock velocity
f_s	pseudo frequency		
h	distance between the wall and the nozzle exit	ψ	wavelet function
		θ	measurement angle with respect to jet axis (free jet) or plate surface(impinging jet)
M	Mach number		
m	order of wavelet function	θ_{Plate}	flat plate installation angle with respect to jet axis
N	feedback loom mode number		
s	wavelet scale	ΔSt	frequency band
St	Strouhal number		

1. INTRODUCTION

The phenomenon of noise generation due to jet impingement is of great concern in transient processes such as short take-off and landing (STOL), vertical take-off and landing (VTOL) aircrafts, and rocket launch vehicles where the emitted high amplitude acoustic waves may result in structural sonic fatigue or electronic components failure (Clarkson, 1994; Jain *et al.,* 2011; Kuizhi *et al.,* 2015). For normal jet impingements, high amplitude

tonal acoustic waves exist in the acoustic spectra at certain nozzle to plate distances and nozzle pressure ratios. This event is described by feedback loop mechanism which appears through the interaction of upstream propagating acoustic waves (generated by the jet-wall interaction) and downstream-travelling coherent flow structures (Krothapalli *et al,.* 1999).

In general, the acoustic field generated by supersonic jet impingement to inclined plates is less investigated compared to the normal jet impingements. Nonomura *et al* (2011). observed three types of
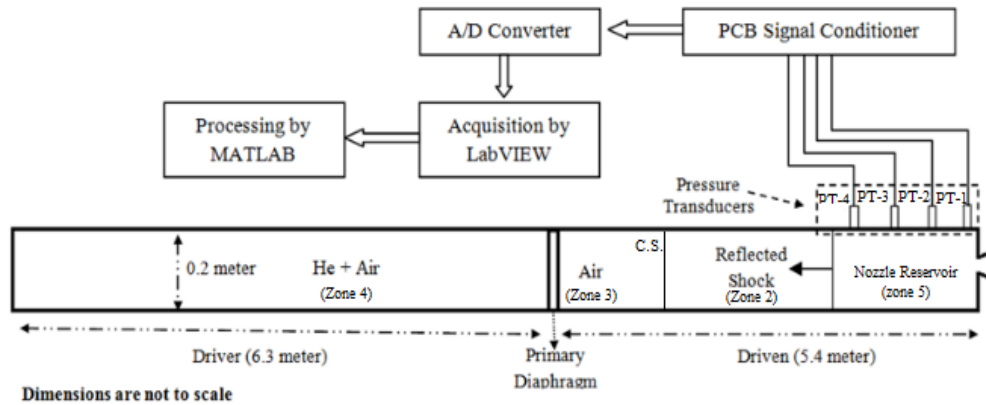
Fig. 1. Schematic illustration of the shock tube facility.

noise sources when an ideally expanded supersonic jet impinges to a 45° inclined plate: Mach waves generated by the jet shear layer before an impingement to the wall, referred to type-A, acoustic waves generated in the impingement region, referred to type-B, and those generated by the wall jet shear layer downstream of the impingement region, referred to type-C (Nonomura, Goto, and Fujii, 2011; Nonomura and Fujii, 2011). It should be mentioned that type-B and type-C acoustic waves have gained more attention due to their potential for greater structural damage.

In addition, while plate inclination angle affects the acoustic wave direction and magnitude in the far-field, the type A, B, and C are observed at different plate inclination angles (Honda *et al.,* 2011). Akamine *et al.* (2014) investigated the far-field acoustic waves of impinging Mach 1.8 cold jet to a 45°. inclined plate where two main propagation direction were observed at θ=30° and θ=75° corresponding to type-C and type-B, respectively. It has been observed that an increase in the jet total temperature will also lead to an enlargement of the supersonic region along the inclined flat plate as well as the development of a thicker wall jet turbulent shear layer (Nonomura, Goto, and Fujii; 2011). Further, a higher SPL for hot jets as well as an increase of the direction angle of both type-B and type-C acoustic waves is observed where the former also intensifies the chances for resonance mode generation. Worden *et al.,* (2013) observed tonal acoustic waves for $M = 1.5$ hot jet impinging to a 45° inclined plate at a distance of $4D$ and $6D$ plate to the nozzle – a distance where the plate is close to the end of the jet potential core (Worden *et al.,* 2013). Signature of type-B is also observed in the far-field (Nonomura, Goto, and Fujii, 2011) indicating the significance of possible upstream propagation of the acoustic waves toward the flying objects and payload. Nevertheless, this phenomenon is not well-modeled in common empirical models for rocket plume noise (Nonomura *et al.,* 2015).

In the case of hot free jets, two distinct types of acoustic waves are observed at the far-field: a peaky, high-amplitude acoustic wave at $30° \leq \theta \leq 45°$ and a flat frequency-spectrum with low-amplitude acoustic

wave at $75° \leq \theta \leq 90°$ (Tam, 1991; Tam, 1996; Hileman *et al.,* 2005; Casalino *et al.,* 2008; Kœnig *et al.,* 2013; Jahromi *et al.,* 2017; Balakrishnan *et al.,* 2018).

The focus of this paper is to explore the development of the acoustic pressure waves when a hot jet impinges to an inclined flat plate. To gain a better insight into the sources of the different types of impinging jet noise, a comparison between the characteristics of acoustic pressure waves (e.g. frequency, directivity and amplitude) of the free jet, which is more investigated, and the oblique jet impingement noise is conducted. On the other hand, a comparison between the noise due to impingement of the jet to an inclined flat plate and the noise due to the impingement of jet to a normal plate with respect to jet axis – feedback loop noise – is made. These comparisons of the acoustic signature of the impinging jet with more known noise sources will help us to gain a better insight into the real sources of the noise.

The required jet is generated by a reflected shock tube with a relatively very low jet noise development (Oertel, 1979; Kirk *et al.,* 2001; Sen *et al.,* 2013; Jahromi *et al.,* 2017). A brief review of the test facility is given in section 2. A comparison of the acoustic waves generated due to oblique- and normal jet impingement is provided in section 3.

2. EXPERIMENTAL DETAILS

According to the direction of the acoustic-wave propagation and the signal frequency characteristics, different types of acoustic waves due to oblique jet impingement to an incline flat plate are categorized in previous studies (i.e. type-A, B, and C).

A shock tube, integrated with a converging-diverging nozzle at the end of the driven tube and a nozzle exit diameter (D) of 0.0254 m generates the required jet at a stagnation temperature and a Mach number of 950 K and 1.4, respectively. Figure 1 shows a schematic illustration of the shock tube. The desired thermodynamic conditions at the nozzle inlet (reservoir section in Fig. 1) are provided by a reflected shock wave. Different shock and reflected

shock strengths are generated through proper helium/air mass fractions at different pressures and temperatures while the driven section is vacuumed to the designed pressure (Jahromi *et al.;* 2017).

Quasi-steady nozzle reservoir pressure is required to have a quasi-steady jet at designed condition. When the shock tube initial condition is specified, all of the thermodynamic properties of the air in the nozzle reservoir can be derived from the shock velocity measured with piezo-sensors by using 1D gas dynamic relations:

$$P_{41} = P_{21}\left[1 - (P_{21} - 1)\alpha_{41}\left(\frac{\beta}{\alpha P_{21} + 1}\right)^{1/2}\right]^{-1/\beta} \quad (1)$$

$$\alpha = \frac{\gamma + 1}{\gamma - 1} \quad (2)$$

$$\beta = \frac{\gamma - 1}{2\gamma} \quad (3)$$

$$\frac{T_5}{T_1} = \frac{\left[2(\gamma_1 - 1)M_s^2 + (3 - \gamma_1)\right]\left[(3\gamma_1 - 1)M_s^2 - 2(\gamma_1 - 1)\right]}{(\gamma_1 + 1)^2 M_s^2} \quad (4)$$

$$\frac{P_5}{P_1} = \left[\frac{\gamma_1 M_s^2 + (\gamma_1 - 1)}{(\gamma_1 + 1)}\right]\left[\frac{\left[(3\gamma_1 - 1)M_s^2 - 2(\gamma_1 - 1)\right]}{(\gamma_1 - 1)^2 M_s^2 + 2}\right] \quad (5)$$

Where:

$$M_s^2 = \left(\frac{V_{is}}{a_1}\right)^2 = \beta(\alpha P_{21} + 1) \quad (6)$$

And,

$$a_1 = \sqrt{\gamma R T_1} \quad (7)$$

According to Eqs. (1) to (7), the required P_{41} to gain the designed jet stagnation temperature (T_5) is specified. The initial driven pressure (P_1) is specified so that when the designed initial and reflected shock waves passes over the driven gas, the designed pressure at nozzle reservoir (P_5) for an ideally expanded jet at M = 1.4 is gained. The length of driver and driven section, the diameter of the shock tube pipe, and the helium/air mass fraction are tailored to have the maximum test time (Jahromi *et al.,* 2017). The test time of quasi-steady pressure and temperature at nozzle reservoir is limited by the arrival of the reflected expansion waves from the end of driver section and is 11 ms in the present study.

The sensitivity analysis – according to Eqs. (1) to (7) and experimental results – indicates that the uncertainty in the thermodynamic properties of the gas in nozzle reservoir (e.g. T_5 and P_5), depends on the uncertainty in incident shock velocity (V_{is}) rather than other parameters such as T_1 and P_1 (Mee, 1993). In other words, the uncertainty in the measurement of V_{is}, determines the total uncertainty of the gas properties in nozzle reservoir. The main source of uncertainty in the V_{is} is the reduction of shock velocity due to viscous effects. To reduce the uncertainty in V_{is} measurement, four piezoelectric pressure transducers – PCB model 102B16 – are used to measure the shock wave velocity as well as the pressure at the nozzle inlet (i.e. PT1 to PT4 in Fig. 1) and the mean value of V_{is} between the sensors is used in the formulas.

The focus of the present study is to investigate the source and characteristics of three types of acoustic waves (i.e. Type-A, B, and C) in oblique jet impingement. The characteristics of these acoustic waves are determined by the directivity and frequency content of acoustic pressure signal. Indeed, acoustic pressure at the far-field of impingement point is measured and investigated at the present study. However, to gain a better insight into the sources of these types, the scalograms of the acoustic pressure waves are produced according to wavelet transform. The scalograms are compared with the more-investigated free jet and normal jet impingement acoustic wave scalograms. Six ¼″ GRAS free-field microphones (model 46BE) are used for the acoustic pressure measurements. The microphones are positioned at the far field of the noise source for both free and impinging jets.

A PCB signal conditioner model 481A03 is used for conditioning the signal from piezoelectric transducers. All the signals from piezo-sensors and microphones are logged by NI 4499 24-bit Data acquisition card with the sampling rate of 204 KHz per channel. MALAB software is used the signal processing.

The uncertainty in the function "F" with respect to the parameter $\emptyset_i$ is defined as:

$$(\delta F)_i = \left[\frac{\partial F}{\partial \phi_i}\right]\delta\phi_i \quad (8)$$

When *F* (i.e. a gas property in nozzle reservoir) is a function of N Parameters:

$$F = F(\phi_1, \dots, \phi_N) \quad (9)$$

And,

$$\phi_i = \phi_{i\,true} + \delta\phi_i \quad (10)$$

Where, $\emptyset_{i\,true}$ is the true value and $\delta\emptyset_i$ is the uncertainty in the parameter $\emptyset_i$. Total uncertainty for the function F is defined as $X_F = \delta F / F$ and is calculated as:

$$X_F = \sqrt{[(X_F)_{\emptyset_1}]^2 + \dots + [(X_F)_{\emptyset_N}]^2} \quad (11)$$

Using the Eqs. (8) to (11) and the uncertainties in sensor calibration charts, the uncertainty in the pressure and temperature measurement at the nozzle inlet is kept below 0.5% and an uncertainty in acoustic measurement with less than 0.5 db is assured. For additional information on the shock tube facility, instrumentation, test procedure, and validation of acoustic results, the reader is referred to a previous paper by the authors (Jahromi *et al.,* 2017).

3. RESULTS

In this section, the far-field acoustic signatures of both the free jet and the impinging jet are studied and compared to each other.

3.1 Free Jet Far-Field Noise Signature

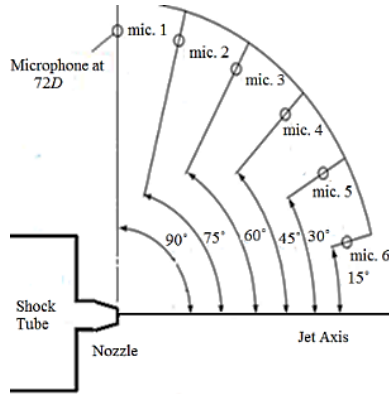Figure 2 illustrates the position of the microphones relative to the nozzle exit for the free jet.

Fig. 2. Position of the microphones relative to the nozzle exit for the free jet.

It should be emphasized that while the acoustic signature consists of a transient starting phenomenon and a quasi-steady jet formation (Oertel, 1979; Lee *et al.,* 2008; Murugan *et al.,* 2008), the focus of this paper is on the latter one (as shown in Fig. 3).

The continuous wavelet transform is used to obtain the energy scalogram of the acoustic waves (Farge, 1992; Kœnig *et al.,* 2010). Continuous wavelet transform of an acoustic signal, *p(t)*, is calculated from Eq. (12) as follows:

$$\tilde{p}(s,t) = \int_{-\infty}^{+\infty} p(\tau)\psi(s,t-\tau)d\tau \tag{12}$$

The parameter "*s*" in Eq. (12) is the scale of the wavelet and "*ψ*" is the "wavelet function" which in this study is a Paul wavelet. Equation (13) determines the Paul function with *m*= 4 (4th order):

$$\psi(1,t-\tau) = \frac{2^m i^m m!}{\sqrt{\pi(2m)!}}\left[1 - i(t-\tau)\right]^{-(m+1)} \tag{13}$$

To compare the results with common FFT frequency spectrums in steady-state facilities, the pseudo-frequency f_s and the correlated Strouhal number *St* are calculated with Eqs. (14) and (15), respectively. In Eq. (15), *D* is the nozzle exit diameter and U_j is the jet velocity (Kœnig *et al.,* 2010).

$$f_s = s(2m+1)/4\pi s \tag{14}$$

$$St = f_s D / U_j \tag{15}$$

The scalograms are the square value of the wavelet transform of the acoustic signal. The dimensionless frequency and the energy of the "acoustic events" are investigated in these scalograms (Kœnig *et al.,* 2010; Jahromi *et al.,* 2017). Acoustic events are acoustic

high energy signals which are determined by using proper mother wavelet in a specific application. Acoustic events are represented as separated parts in scalograms. These parts have three characteristics: the time of occurrence, the maximum frequency, and the frequency band which is indicated by ΔSt. Figure 4 compares the acoustic scalogram of free jet in the present study with the sound pressure level (SPL) frequency spectrum of steady state experiment conducted by Tanna *et al.* (1976) for *M* = 1.4 and T_t = 950 K free jet at $\theta = 45°$.

ΔSt is the frequency band which covers 60% of the maximum sound energy. The frequency of maximum energy in scalogram in the present study is in agreement with the frequency of maximum SPL from steady-state experiments. This outcome confirms that the frequency distribution of acoustic energy in the present pulse facility is in agreement with those from steady-state investigations.

3.2 Impinging Jet

3.2.1 Oblique Jet Impingement

Figure 5 illustrates the position of the microphones and the different acoustic wave types for the oblique jet impingement to a 45˚ inclined flat plate.

Figure 6 (a) to (f) illustrates the acoustic pressure signal for the microphones at $\theta =15°$, 30°, 45°, 60°, 75°, and 90˚ of the oblique jet impingement to a 45˚ inclined plate (θ_{Plate} = 45°). The time span of 150<*tU/D*<260, marked with dashed lines, represents the sound wave due to the quasi-steady jet impingement to the wall and is the objective of the present study.

Overall Sound Pressure Level (OASPL) of the quasi-steady jet in Fig. 6 for all the microphones is illustrated in Fig. 7(a). High amplitude acoustic waves at $\theta = 45°$ and $\theta = 60°$ (type-C acoustic wave) and θ=75˚ (type-B acoustic wave) are observed in Fig. 7(a). It should be emphasized that while the value of the present results might differ from previous investigations; however, the behavior are very similar and obey the same path– as Fig. 7(b) that is a result of a numerical investigation on the noise of oblique jet impingement to a flat plate shows (Nonomura, Goto, and Fujii, 2011).

Figure 8 (a) to (f) compares the scalograms of 60% retained energy of the maximum acoustic energy and the related frequency band (ΔSt) for quasi-steady free jet (left column) and quasi-steady zone of the acoustic signal in oblique jet impingement (right column) at $\theta =15°$, 30°, 45°,60°,75°, and 90°.

Acoustic scalograms at $\theta = 15°$, 30°, 45° and 60° shows that the Strouhal number of the maximum energy and ΔSt of jet impingement to 45˚ inclined plate are very close to the maximum energy Strouhal number and ΔSt of the free jet. Further, results indicate of the existence of intermittent acoustic events related to jet mixing layer at these angles (Kœnig *et al.,* 2010; Jahromi *et al.,* 2017). This phenomenon is also in agreement with previous findings and states that the source of type-C acoustic wave is the wall jet shear layer at the downstream of the impingement region.
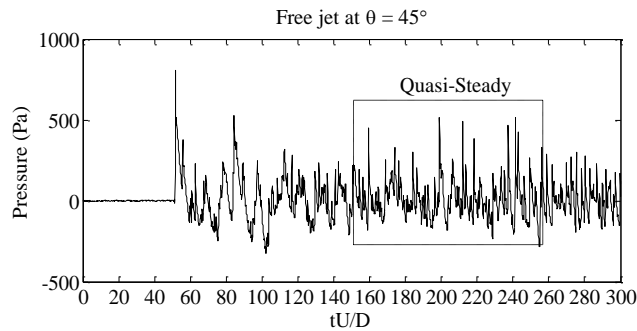
Fig. 3. Acoustic signature of the free jet at θ =45° (data from mic.4 in Fig. 2).

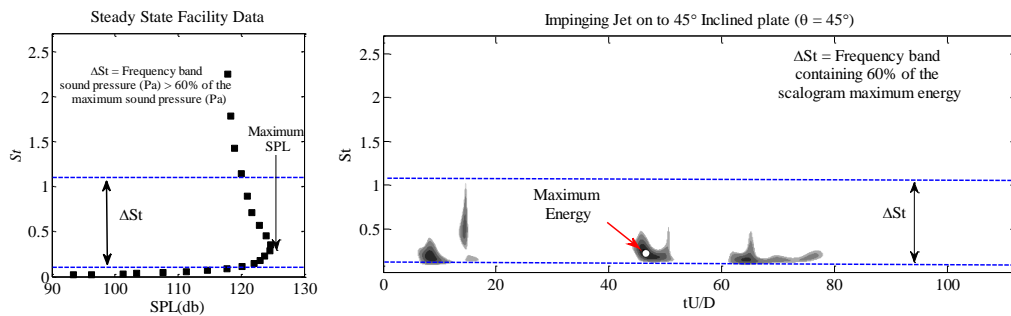**Fig. 4. Scalogram of acoustic pressure signal of the mic.4 (θ=45°) of free jet in present study (right column) and the SPL frequency spectrum of a free jet generated by a steady-state facility (Tanna *et al.,* 1976) at *M*=1.4 and T_t=950 K (left column).**
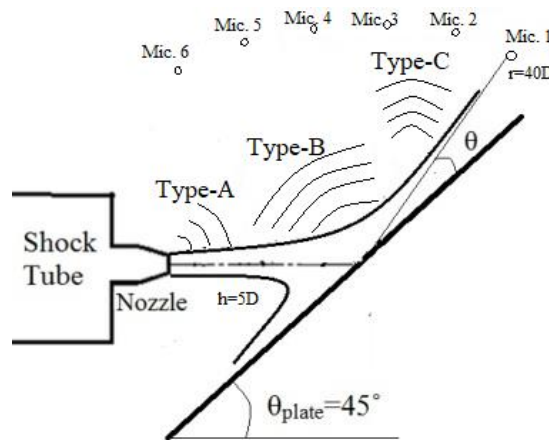

Fig. 5. Position of the microphones at the oblique jet impingement to a 45° inclined plate.

However, at θ=75° (Fig. 8(e)) and θ=90° (Fig. 8(f)), the acoustic events in the free jet differ from those by the impinging jet. At θ=75°, a narrowband (low ΔSt), non-intermittent, and low frequency (maximum St number ≈ 0.15) tonal acoustic signature is seen for the oblique impingement. The appearance of acoustic signature at a distinct acoustic frequency resembles a resonance mode in the feedback loop mechanism (Krothapalli *et al.,* 1999).

3.2.2 Normal Jet Impingement

The far-field acoustic signature of the normal jet impingement to the wall is investigated to understand the noise source due the jet/wall interaction. Figure 9 illustrates the position of the microphones for normal jet impingement. The acoustic waves, induced by normal jet impingement to the plate, are seen at low polar angles at the far-field of the impinging point (Shen *et al.,* 1993).

Figure 10 illustrates the far-field acoustic pressure signal for the microphones positioned at θ = 15° of the jet impingement normal to the flat plate. The quasi-steady jet for the time zone of interest is considered. A harmonic resonance mode is seen at θ= 15°. Resonance or feedback loop phenomenon is

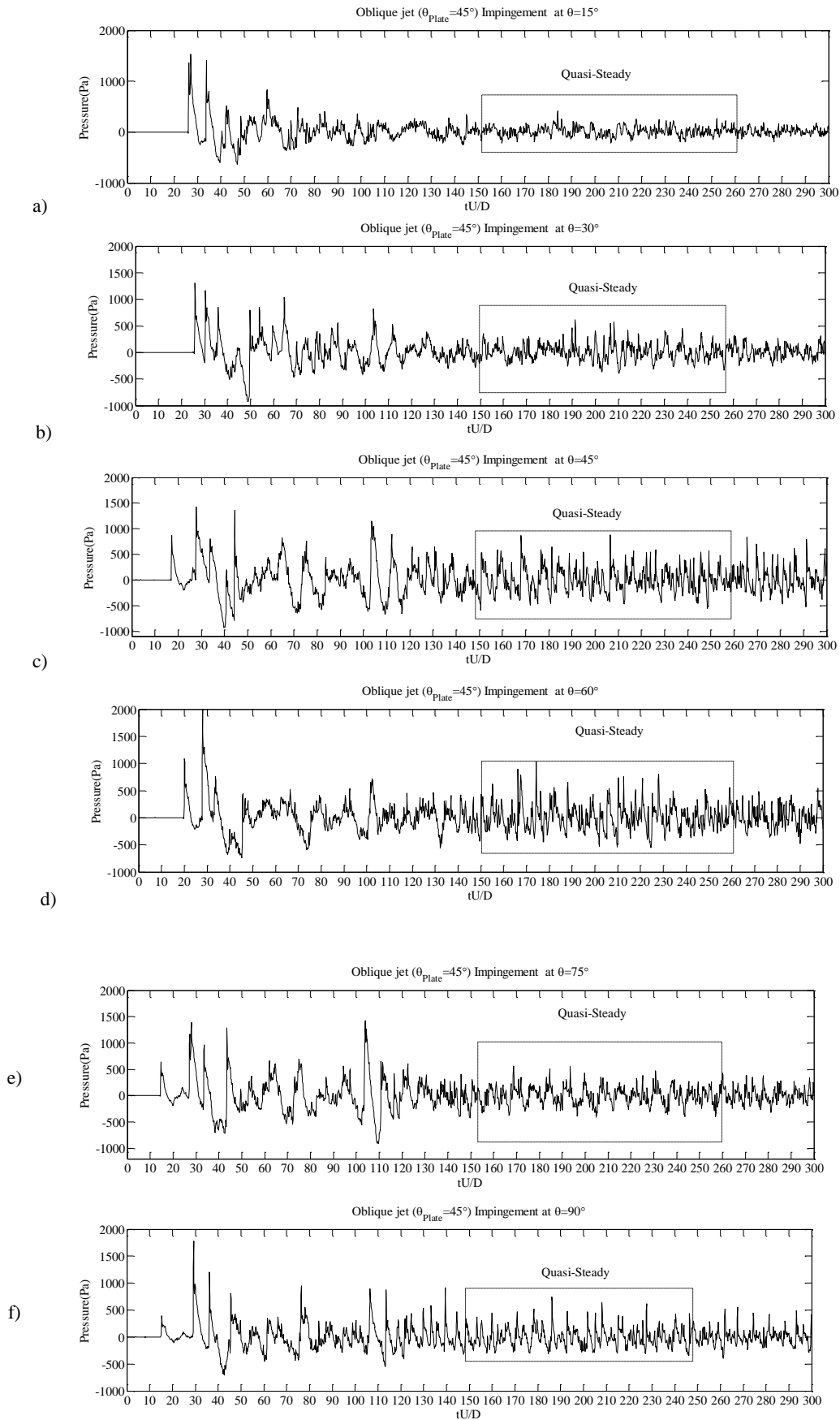**Fig. 6. The acoustic pressure signal for microphones at a) θ=15˚, b) θ=30°, c) θ=45°, d) θ=60°, e) θ=75°, and f) θ=90° of the oblique jet impingement to a 45˚ inclined plate.**
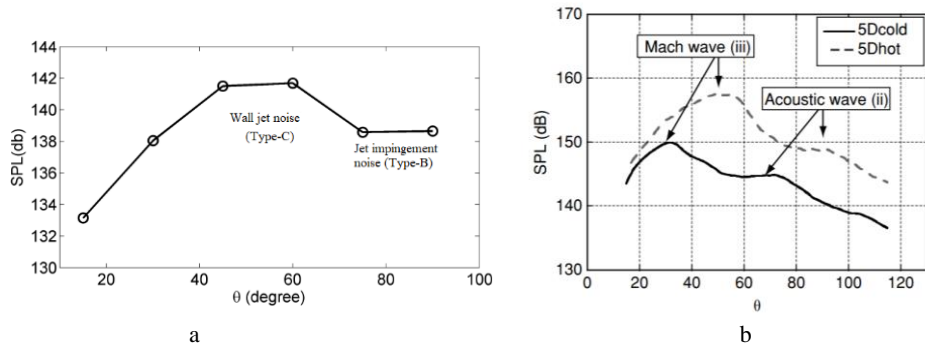
a

b

Fig. 7. OASPL of the oblique jet impingement to a 45° inclined plate at different polar angles a) present study b) result of Nonomura, Goto, and Fujii (2011).
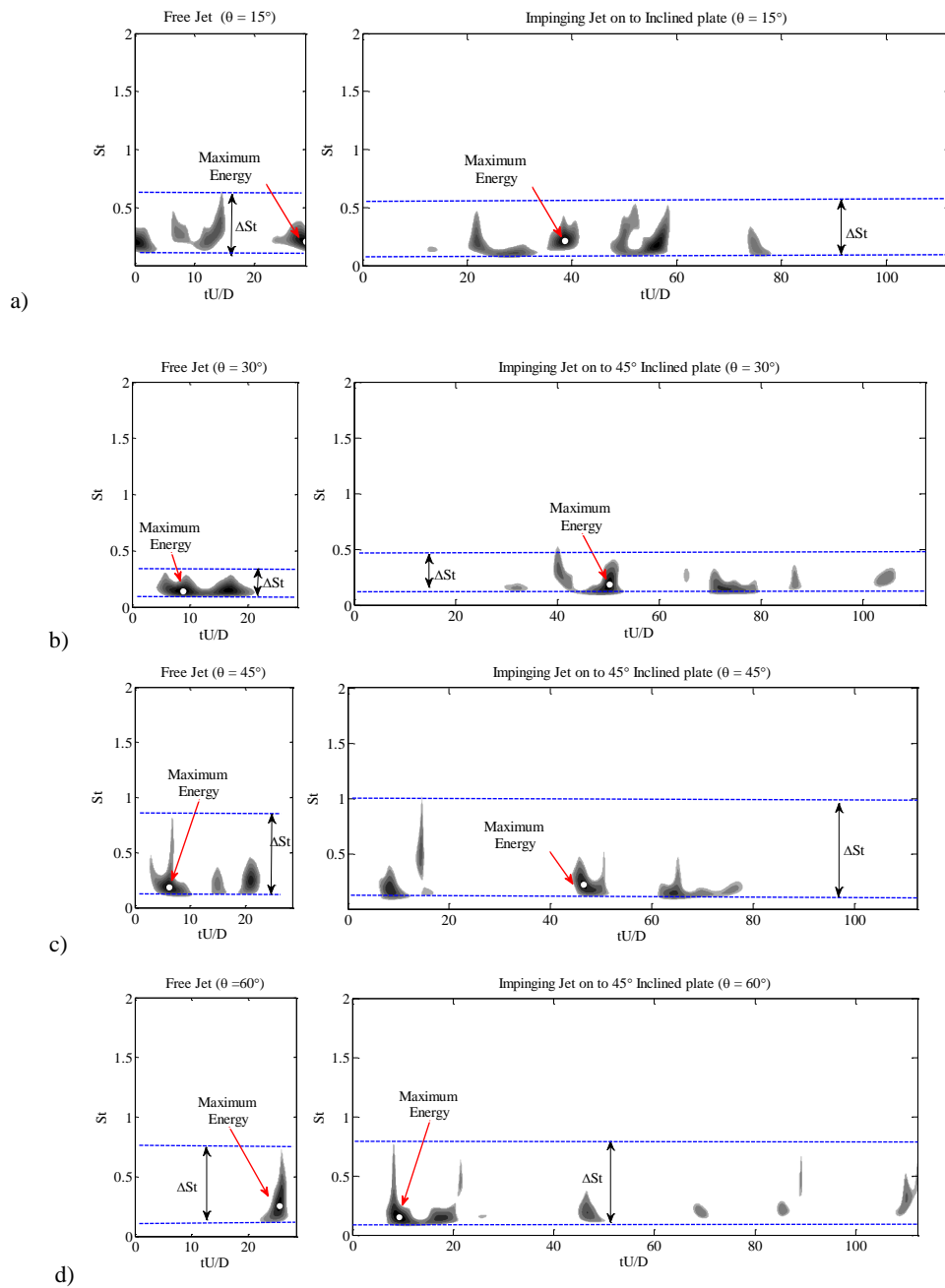

Fig. 8. Scalogram of acoustic pressure signal of quasi- steady free jet (left) and oblique jet impingement to a 45° inclined plate (right) at a) θ=15°, b)θ=30° c) θ θ=45° d)θ=60°, e)θ=75° and f)θ=90°.
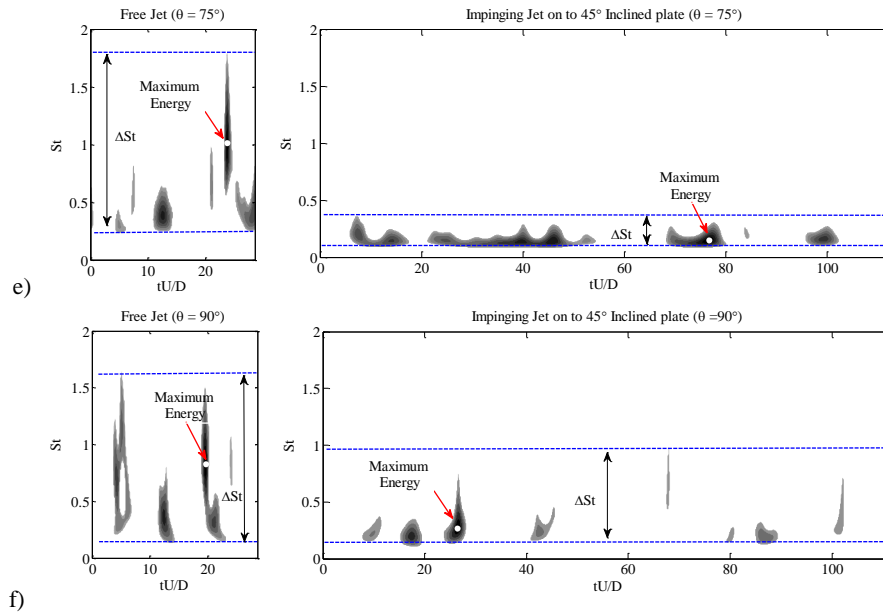
Fig. 8. Continued.

widely accepted for normal impinging jets (Krothapalli *et al.,* 1999). However, the source of noise sources for oblique jet impingement – specially type-B acoustic wave – is not well determined yet. At the present study, a tonal acoustic wave (i.e. at specific frequency) in oblique jet impingement represents the type-B acoustic signal. Previous studies show that in normal jet impingement a tonal acoustic wave exists. According to this similarity, a comparison between the characteristics of acoustic signal type-B in oblique jet impingement and the signal due to feedback loop mechanism is made. A comparison of the acoustic waves at the far-field of normal impingement with the noise due to the oblique impingement discloses a better understanding of the source of the type-B acoustic wave in oblique jet impingement.

Fig. 9. Position of the microphones for normal jet impingement.

In the case of normal jet impingement, if the wall is close to the end of the jet potential core then the wall/jet interaction noise of high speed jets is observed more at low polar angles relative to the wall (Shen *et al.,* 1993). Figure 11 compares the scalogram of the acoustic waves for normal jet impingement at $\theta = 15°$ (mic.1 shown in Fig. 11(a)) and oblique jet impingement at $\theta = 75°$ (mic.5 shown in Fig. 11(b)) at the far-field of the impinging point.

It is seen that the acoustic wave for oblique jet impingement at $\theta = 75°$ (type-B acoustic wave) is similar to the traditional tonal noise in normal jet impingement which is due to jet/wall interaction.

The maximum energy of the resonance mode at $\theta =75°$ for oblique impingement and $\theta=15°$ for normal impingement occurs at $St = 0.15$. From Eq. (15), the pseudo frequency for this St Number is f_s=4215 (Hz). The tone frequency f_N associated with the feedback loop mechanism in normal jet impingement is governed from the following formula (Powell, 1988):

$$\frac{N \pm p}{f_N} = \int_0^h \left(\frac{dh}{C_i} + \frac{dh}{C_a} \right) \tag{16}$$

Where C_i is the convection velocity of the large scale structures in the jet shear layer, C_a is the acoustic wave velocity, h is the distance between the nozzle and the flat plate, N is the feedback loop mode, and p is the phase lag between the acoustic waves ($p = 0$ when there is no lifting surface around the nozzle exit (Krothapalli *et al.,* 1999)). It should be pointed out that $C_i = 0.52U$ is recommended (Krothapalli *et al.,* 1999). Considering N=3 in Eq. (16), the resonance frequency is determined as f_3=4237 (Hz) which is in excellent agreement with the resonance frequency f_s=4215 (Hz) observed in scalograms of Fig. 11.
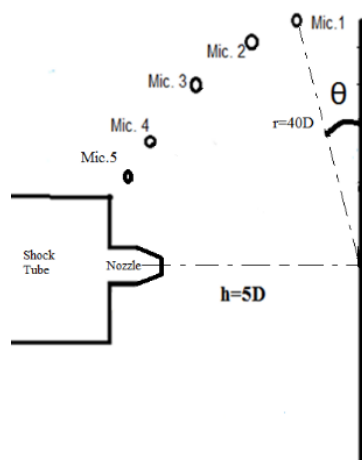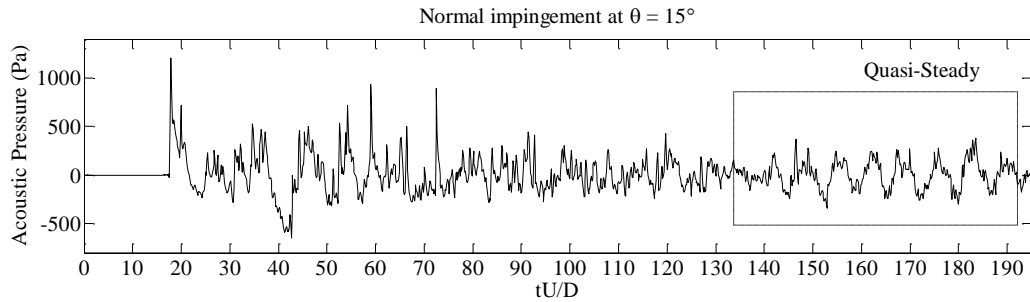
Fig. 10. Far-field acoustic pressure signal for the microphone positioned at *θ*=15° of normal jet impingement to the flat plate.

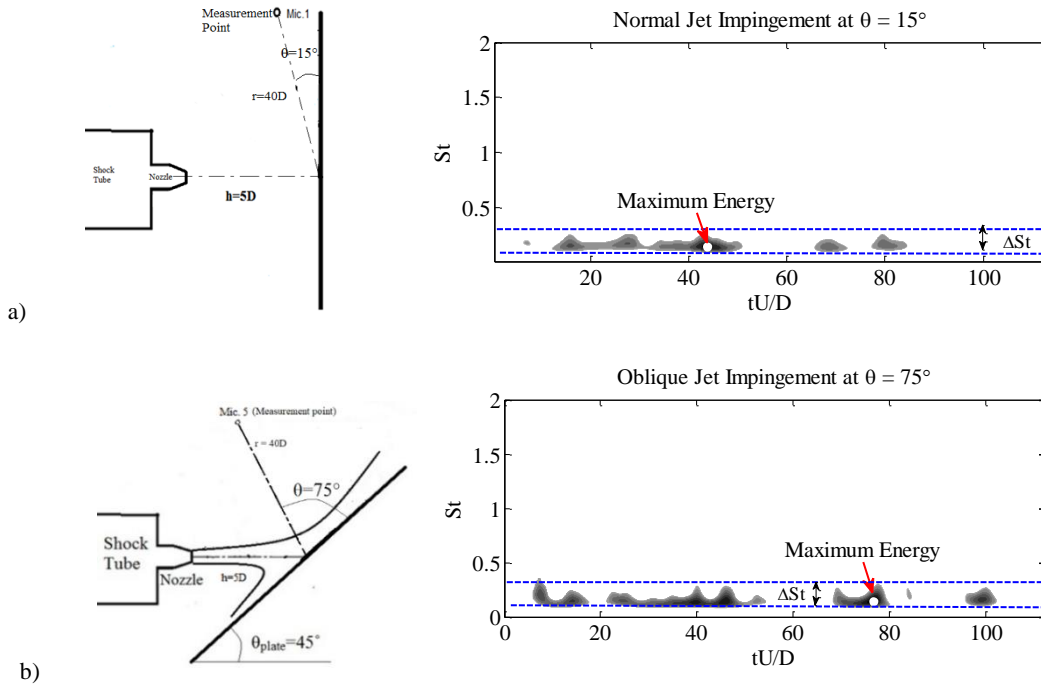**Fig. 11. Scalogram of the acoustic waves for a) normal jet impingement at *θ*=15° and b) oblique jet impingement at *θ*=75° at the far-field of the impinging point.**

4. CONCLUSION

Acoustic waves due to jet impingement on a 45° inclined plate are investigated. A pulse facility is designed and employed to generate a supersonic hot jet at $M = 1.4$ and $T_t = 950$ Kelvin. The OASPL of the acoustic signal for oblique impingement show strong acoustic waves at $\theta = 45°$ (type-C acoustic wave) and $\theta = 75°$ (type-B acoustic wave) which is compatible with previous results on hot impinging jets. Continuous wavelet transform is used to analyze the acoustic signals for both the free- and impinging jets. The scalograms of impinging jet to an inclined plate are compared with those of free jet and normal jet impinging. It is observed that, for oblique impingement, the acoustic events at $\theta = 15°, 30°, 45°$ and $60°$ (type-C acoustic waves) are very similar to the free jet noise signature at the same polar angles and are generated by wall/jet mixing shear layer. A resonance shape wave is observed at $\theta = 75°$ which exists in normal jet impingement at $\theta = 15°$. The signal scalogram at $\theta = 15°$ for normal jet impingement is compared with the scalogram of

oblique jet impingement at $\theta = 75°$. The acoustic scalogram at these polar angles are similar and supporting the fact that the source of these acoustic waves is the jet/plate interaction and the propagation direction of this acoustic wave depends on the plate inclination angle. Finally, it is determined that for normal jet impingement, the frequency of the resonance is similar to the frequency of the third mode of the feedback loop mechanism.

REFERENCES

Akamine, M., Y. Nakanishi, K. Okamoto, S. Teramoto, T. Okunuki and S. Tsutsumi (2014). Experimental study on acoustic phenomena of supersonic jet impinging on inclined flat plate. *Proceedings of the 52nd Aerospace Sciences Meeting,* National Harbor, Maryland, United states, 0879.

Balakrishnan, P. and K. Srinivasan (2018). Influence of swirl number on jet noise reduction using flat vane swirlers. *Aerospace Science and*

Technology 73, 256-268.

Casalino, D., F. Diozzi, R. Sannino and A. Paonessa (2008). Aircraft noise reduction technologies: a bibliographic review. *Aerospace Science and Technology* 12 (1), 1-17.

Clarkson, B. L. (1994). *Review of sonic fatigue technology.* NASA Report, NASA-CR-4587.

Farge, M. (1992). Wavelet transforms and their applications to turbulence. *Annual review of fluid mechanics* 24 (1), 395-458.

Hileman, J. I., B. S. Thurow, E. J. Caraballo and M. Samimy (2005). Large-scale structure evolution and sound emission in high-speed jets: real-time visuali-zation with simultaneous acoustic measurements. *Journal of Fluid Mechanics* 544, 277-307.

Honda, H., T. Nonomura, K. Fujii and M. Yamamoto (2011). Effects of Plate Angles on Acoustic Waves from a Supersonic Jet Impinging on an Inclined Flat Plate. *Proceedings of the 41st AIAA Fluid Dynamics Conference and Exhibit,* Honolulu, Hawaii, U.S.A., 3260.

Jahromi, I. B., M. Ebrahimi and K. Ghorbanian (2017). Reflected shock tube experiments on aeroacoustic signature of hot jets. *Journal of Mechanical Science and Technology* 31(8), 3811-3820.

Jain, P. C., A. Mukherjee and Y. Krishna (2011). Tuned mass dampers for flight vehicle components subjected to rocket noise. *Aerospace Science and Technology* 15 (3), 175-182.

Kirk, D. R., D. O. Creviston, I. A. Waitz (2001). Aeroacoustic measurement of transient hot nozzle flows. *Journal of Propulsion and Power* 17(4), 928-935.

Koenig, M., A. Cavalieri, P. Jordan, J. Delville, Y. Gervais, D. Papamoschou, M. Samimy and S. Lele (2010). Far field filtering and source imaging for the study of jet noise. *Proceedings of the 16th AIAA/CEAS Aeroacoustics Conference,* Stockholm, Sweden, 3779.

Kœnig, M., A.V. Cavalieri, P. Jordan, J. Delville, Y. Gervais and D. Papamoschou (2013). Far field filtering and source imaging of subsonic jet noise. *Journal of Sound and Vibration* 332(18), 4067-4088.

Krothapalli, A., E. Rajkuperan, F. Alvi and L. Lourenco (1999). Flow field and noise characteristics of a supersonic impinging jet. *Journal of Fluid Mechanics* 392, 155-181.

Kuizhi, Y., C. Liangliang, L. Hu and W. Yunliang (2015). Analysis of jet blast impact of embarked aircraft on deck takeoff zone. *Aerospace Science and Technology* 45, 60-66.

Lee, C. and D.J. Lee (2008). An analysis of flow and screech tone from supersonic axisymmetric jet at the initial stage. *Journal of Mechanical Technology* 22(4), 819-826.

Mee, D. J. (1993). *Uncertainty analysis of conditions in the test section of the T4 shock tunnel.* The University of Queensland. Report No. 4/93.

Murugan, T. and D. Das (2008). On evolution and acoustic characteristics of a compressible vortex ring. *International Journal of Aeroacoustics* 7(3-4), 199-222.

Nonomura, T. and K. Fujii (2011). Computational study of effects of near-wall turbulent structure on aeroacoustic waves from a supersonic jet impinging on an inclined plate. *Proceedings of the 17th AIAA/CEAS Aeroacoustics Conference*, Portland, Oregon, 2917.

Nonomura, T., H. Honda, Y. Nagata, M. Yamamoto, S. Morizawa, S. Obayashi and K. Fujii (2015). Plate-Angle Effects on Acoustic Waves from Super-sonic Jets Impinging on Inclined Plates. *AIAA Journal* 54 (3), 816-827.

Nonomura, T., Y. Goto and K. Fujii (2011). Aeroacoustic waves generated from a supersonic jet impinging on an inclined flat plate. *International Journal of Aeroacoustics* 10(4), 401-425.

Oertel, H. (1979). Kinematics of Mach waves inside and outside supersonic jets. *Recent Developments in Theoretical and Experimental Fluid Mechanics* 121-136.

Powell, A. (1988). The sound‑producing oscillations of round underexpanded jets impinging on normal plates. The *Journal of The Acoustical Society of America* 83 (2), 515-533.

Sen, H.O., F. Seiler and J. Srulijes (2013). Visualization of Mach waves produced by a supersonic jet and theoretical explanations. *Journal of Visualization* 16(4), 303-312.

Shen, J. and W.C. Meecham (1993). Quadrupole directivity of jet noise when impinging on a large rigid plate. *The Journal of the Acoustical Society of America* 94(3), 1415-1424.

Tam, C.K. (1991). Jet noise generated by large-scale coherent motion. *Aeroacoustics of Flight Vehicles: Theory and Practice* 1.

Tam, C.K., M. Golebiowski and J.M. Seiner (1996). On the two components of turbulent mixing noise from supersonic jets. *Aeroacoustics Conference*, PA, U.S.A., 1716, State College.

Tanna, H., P.D. Dean and R.H. Burrin (1976). *The generation and radiation of supersonic jet noise.* AFAPL-TR-76-65- Vol III.

Worden, T.J., J.P. Gustavsson, C. Shih and F.S. Alvi (2013). Acoustic Measurements of High-Temperature Supersonic Impinging Jets in Multiple Configurations. *Proceedings of the 19th AIAA/CEAS Aeroacoustics Conference,* Berlin, Germany, 2187.